Journal of Power Sources 198 (2012) 308–311

Contents lists available at SciVerse ScienceDirect

Journal of Power Sources

journal homepage: www.elsevier.com/locate/jpowsour

Short communication

Nano $LiMn_2O_4$ as cathode material of high rate capability for lithium ion batteries

W. Tang[a,b], X.J. Wang[a], Y.Y. Hou[a], L.L. Li[a], H. Sun[a], Y.S. Zhu[a], Y. Bai[b], Y.P. Wu[a,*], K. Zhu[b,*], T. van Ree[c,**]

[a] New Energy and Materials Laboratory (NEML), Department of Chemistry & Shanghai Key Laboratory of Molecular Catalysis and Innovative Materials, Fudan University, Shanghai 200433, China
[b] Shanghai Institute of Space Power-Sources (SISP), Shanghai Academy of Spaceflight Technology, Shanghai 200233, China
[c] Department of Chemistry, University of Venda, Thohoyandou 0950, South Africa

ARTICLE INFO

Article history:
Received 21 August 2011
Received in revised form
26 September 2011
Accepted 29 September 2011
Available online 5 October 2011

Keywords:
Lithium ion batteries
$LiMn_2O_4$
Nanochain
Rate capability

ABSTRACT

A nanochain of $LiMn_2O_4$ was prepared by a sol–gel method using an aqueous solution of metal salts containing starch. Its electrochemical behavior was characterized by cyclic voltammography, capacity measurement and cycling performance. The results obtained show that the nanochain $LiMn_2O_4$ cathode has a very good rate capability. It shows a reversible capacity of 100 mAh g^{-1} at 100 mA g^{-1} (about 1 C) and 58 mAh g^{-1} even at a charge rate of 20 C. In addition, when the cathode is charged at 1 C, 70 mAh g^{-1} (70% capacity at 1 C) can be achieved even at a discharge rate of 50 C, with a cut-off voltage of 3.0 V in 1 M $LiClO_4$ solution of EC/DEC/DMC (1:1:1, v/v/v). Furthermore, the cycling behavior of the cathode is also very satisfactory. This suggests that this nanochain $LiMn_2O_4$ has great promise for practical application as high rate cathode material for lithium ion batteries.

1. Introduction

Electric vehicles (EV) using rechargeable lithium ion batteries are regarded as one efficient way to solve two great problems of industrialization: the shortage of oil sources and the pollution of the environment [1–3]. The development of lithium ion batteries with high energy density at high power is the key to the success of EV technology [1] and has recently become an attractive topic for both scientific and industrial interests [4–7].

When the capacity of the batteries becomes large enough to meet the energy required for EVs and HEVs, their safety is a crucial problem. Two lithium intercalation compounds, olivine $LiFePO_4$ and spinel $LiMn_2O_4$, have received particular attention due to their better safety [8–17]. The latter has been studied as cathode material for many years since it exhibits a potential of 4.0/4.2 V versus Li^+/Li when cycled over the composition range of $Li_xMn_2O_4$ ($0 < x < 1$) and presents higher thermal stability than the widely used $LiCoO_2$ [13,17], and is safer and more suitable for large capacity devices. On the other hand, although spinel $LiMn_2O_4$ has many advantages, its low electrical conductivity has been considered a limiting factor for applications requiring high power [1]. Taking these two aspects into account, nano-structured $LiMn_2O_4$ materials have shown promise with improved electrochemical performance such as high rate capability and long cycling life over their bulk counterparts due to the large electrode/electrolyte interface and shorter Li^+ diffusion path length [7,18–20,6,21–25].

In our current work, a nanochain $LiMn_2O_4$ with beads of 100 nm was prepared using a starch-assisted sol–gel method. A special microstructure was obtained, while the particle size could be reduced into the nano range. Previously, several two-step methods have been applied to create such a structure [7,34–36] and in our work this novel structure could be obtained in a one-step reaction, which could be more convenient and cheaper. We have found that the electrode can deliver a reversible capacity of 100 mAh g^{-1} at 1 C and excellent high rate capability in a $LiClO_4$-based electrolyte [17]. This is about 80% of its theoretical rate capability, 148.2 mAh g^{-1}, which seems to be due to the use of $LiClO_4$ electrolyte. Its cycling behavior is also very good because of the unique nanochain structure.

2. Experimental

All the reagents were analytical grade. $LiMn_2O_4$ nanochains were synthesized by a starch-assisted sol–gel method. In a typical synthesis, 0.4 g starch was placed in a water-free flask and 25 ml distilled H_2O was added into the flask. The resultant mixture was heated initially at 110 °C until the solution became transparent, while stirring (marked as solution A). Then 5 mmol manganese nitrate (0.895 g as a 50% solution) and 2.5 mmol lithium nitrate (0.1724 g) were added together and dissolved to get a

* Corresponding author.
** Corresponding author. Tel.: +27 15 9628262; fax: +27 15 9624749.
E-mail addresses: wuyp@fudan.edu.cn (Y.P. Wu), zhukai811@sina.com (K. Zhu), Teuns.VanRee@univen.ac.za (T. van Ree).

0378-7753/$ – see front matter © 2011 Elsevier B.V. All rights reserved.
doi:10.1016/j.jpowsour.2011.09.106

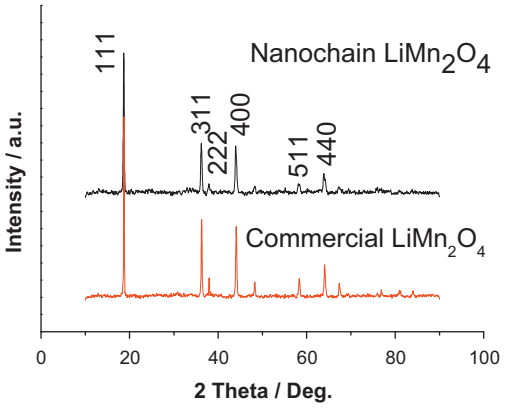

Fig. 1. X-ray diffraction patterns of the nanochain and commercial $LiMn_2O_4$.

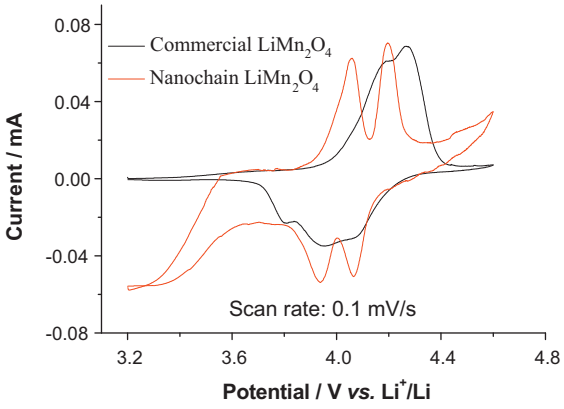

Fig. 3. CV curves of the nanochain and commercial $LiMn_2O_4$ at the scan rate of 0.1 mV s^{-1} using Li metal as the counter and reference electrode.

homogeneous solution (marked as solution B). Solution B was added into solution A while stirring and then the mixture was kept at 110 °C for 1.5 h. The resultant mixture was dried initially at 110 °C for 12 h to get a precursor in the form of foam. The dried foam was put into a muffle oven and heated to 750 °C at a heating rate of 2 °C min^{-1} over 5 h to obtain $LiMn_2O_4$ nanochains [25]. After being powdered, the obtained particles were analyzed by X-ray diffraction on a Bruker D4 X-ray diffractometer with Ni-filtered CuK_α radiation. For comparison, a commercial $LiMn_2O_4$ sample was purchased from Shanshan Company (China) and used as received without further treatment.

A scanning electron micrograph (SEM) was obtained on a Philips XL 30 scanning electron microscope, and transmission electron micrographs (TEM) were recorded on a JEOL JEM-2010 transmission electron microscope.

The as-prepared $LiMn_2O_4$ and commercial $LiMn_2O_4$ were each mixed with acetylene black and poly(tetrafluoroethylene) (PTFE) in a weight ratio of 7.5:1.5:1, respectively, with the help of ethanol. After drying, the mixture was pressed into a film, and then the film was cut into disks of about 1.5 mg and 0.4 cm^2. These disks were pressed onto Ni grid at a pressure of 10 MPa and then dried at 120 °C overnight to act as working electrodes. The CV data of the $LiMn_2O_4$ electrodes were collected on a CHI660C electrochemical workstation (Chenhua, China) and charge/discharge behaviors were measured in coin-type cells using a LANDct3.3 battery tester. The electrolyte was 1 M $LiClO_4$ dissolved in ethylene carbonate (EC): diethyl carbonate (DEC): ethyl methyl carbonate (DMC) at a 1:1:1 volume ratio. A porous polypropylene (PP) film (Cellgard 2400) was used as the separator.

3. Results and discussion

XRD patterns of the as-prepared and commercial $LiMn_2O_4$ are shown in Fig. 1. The diffraction peaks at 18.66°, 36.30°, 38.06°, 44.1°, 48.3°, 58.21°, 63.80° and 67.38° are indexed to the spinel $LiMn_2O_4$ and these values are close to those reported in the JCPDS data (JCPDS file No. 35-0782). The intensities of the XRD peaks for the as-prepared $LiMn_2O_4$ are weaker than those for the commercial $LiMn_2O_4$.

Morphology of the as-prepared nanochain and commercial $LiMn_2O_4$ is shown in Fig. 2. The mechanism of formation needs further investigation, but it is assumed that the starch chain structure played a decisive role in formation of the $LiMn_2O_4$ nanochains. Our prepared $LiMn_2O_4$ exists in the nanochain shape, and consists of beads of about 100 nm diameter. This type of interconnected nanocrystalline morphology may help the transferring process of Li^+ ions and allow a better rate performance [16] while the commercial $LiMn_2O_4$ materials are bulk particles that consist of aggregated submicron-sized particles (on the average about 200–300 nm).

The CV curves of the nanochain and commercial $LiMn_2O_4$ at a scan rate of 0.1 mV s^{-1} in a potential range of 3.0–4.6 V (*vs.* Li/Li^+) are shown in Fig. 3. The nanochain $LiMn_2O_4$ shows two pairs of clearly separated sharp redox peaks. The oxidation peaks are located at 4.06 and 4.19 V and the corresponding reduction peaks are located at 3.94 and 4.06 V, respectively. These values are close to those reports corresponding to lithium ion removal from the tetrahedral sites in the spinel. In the case of the commercial $LiMn_2O_4$, although the two pairs of redox peaks are very clear, the separation of the peaks is not very clear. This suggests that the nanochain $LiMn_2O_4$ will present better redox behavior due to the special micro–nano nature of the material [24,25].

Nyquist plots of the nanochain and commercial $LiMn_2O_4$ using Li metal as the counter electrode are shown in Fig. 4. It can be seen clearly that the charge transfer resistance (R_{ct}) of the nanochain $LiMn_2O_4$ is much lower than that of the commercial one. This indicates that the rate capability of the nanochain $LiMn_2O_4$ will be better than that of the commercial one. This is presumably mainly

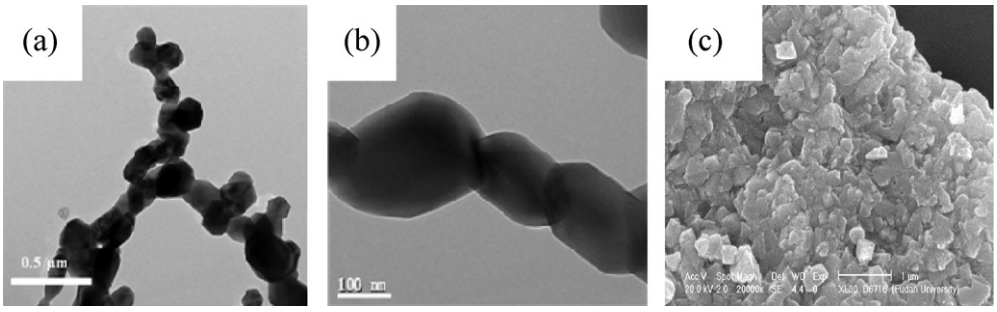

Fig. 2. (a) and (b) TEM micrographs of the as-prepared nanochain $LiMn_2O_4$; and (c) SEM micrograph of commercial $LiMn_2O_4$.

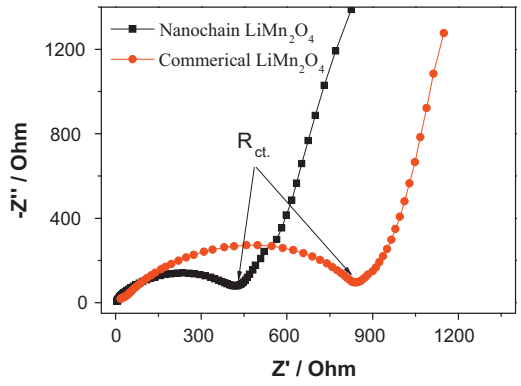

Fig. 4. Nyquist plots of the nanochain and commercial $LiMn_2O_4$ using Li metal as the counter electrode between 3 and 4.6 V.

due to the shorter diffusion path and higher surface area for the nanochain $LiMn_2O_4$ than that for the commercial one.

Charge and discharge curves of the nanochain $LiMn_2O_4$ at different rates and capacities at different rates for the nanochain and commercial $LiMn_2O_4$ by using Li metal as the counter electrode are shown in Fig. 5. The charge and discharge rates at different cycles for the nanochain $LiMn_2O_4$ electrode are the same, and the rates are controlled as follows: 1 C for the first to the fourth cycles, 2 C for the fifth to the seventh ones, 5 C for the eighth to the eleventh ones, 10 C for the twelfth and thirteenth ones, 20 C for the fourteenth to sixteenth ones and 1 C again for the seventeenth to twentieth cycles. As expected, the charge and discharge capacities decrease with an increase in the rate. The reversible capacities of the nanochain $LiMn_2O_4$ are 100, 99.8, 93.5, 81.7 and 58 mAh g^{-1} at 1 C, 2 C, 5 C, 10 C and 20 C, respectively. At the rate of 20 C, 58% of the discharge capacity in the first cycle is reserved and 96% of the

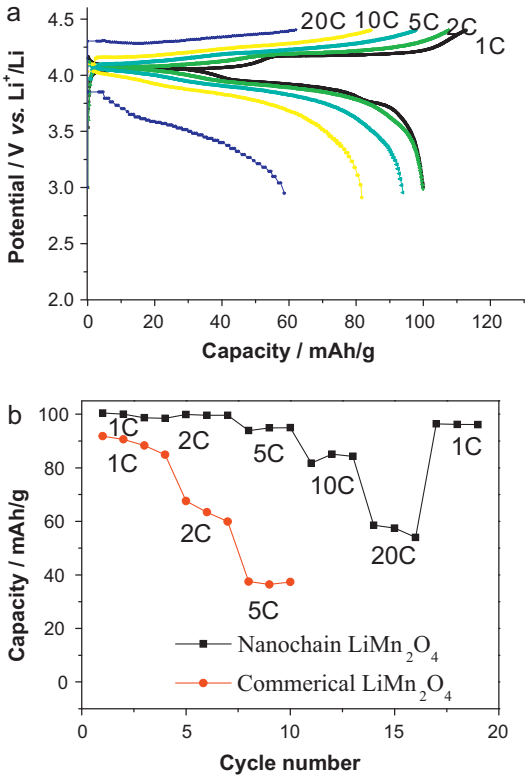

Fig. 5. (a) Charge and discharge curves of the nanochain $LiMn_2O_4$ at different rates and (b) capacities at different rates for the nanochain and commercial $LiMn_2O_4$ using Li metal as the counter electrode.

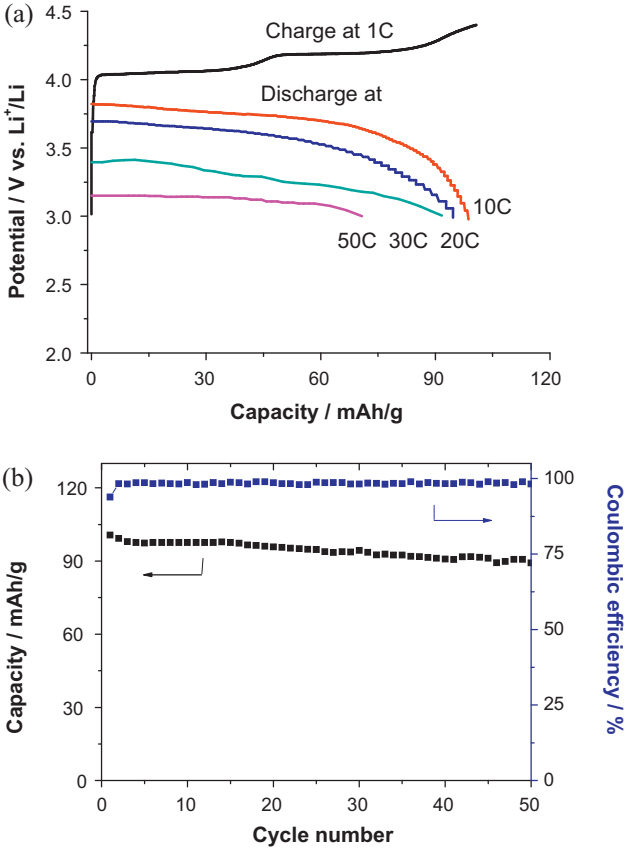

Fig. 6. (a) Discharge curves at different rates when the charge rate is 1 C and (b) cycling behavior for the nanochain $LiMn_2O_4$ at the current density of 200 mA g^{-1} (2 C) using Li metal as the counter electrode.

discharge capacity in the first cycle is recovered when the rate comes back to 1 C again. In contrast, the commercial $LiMn_2O_4$ presents a reversible capacity of 92 mAh g^{-1} at 1 C due to the doping to avoid the Jahn–Teller effects leading to poor cycling [26]. However, when the charge and discharge rate reaches 5 C, only 36 mAh g^{-1} is reserved. Evidently, the excellent rate capability is due to the nanochain structure of $LiMn_2O_4$, which is consistent with the above results from the CV curves and Nyquist plots.

As to the nanochain $LiMn_2O_4$, at the rate of 1 C, two voltage plateaus at about 4 V can be identified from the charge and discharge curves. This is consistent with its CV curves shown in Fig. 3. When the rate increases, the two plateaus combine together and the discharge voltage decreases due to the increase of overpotentials.

Fig. 6 displays discharge curves at different rates when the charge rate is 1 C, and cycling behavior for the nanochain $LiMn_2O_4$ at the current density of 200 mA g^{-1} (2 C), using Li metal as the counter electrode. When the nanochain $LiMn_2O_4$ electrode is charged at 1 C rate and then discharged at 10 C, 20 C, 30 C and 50 C, respectively, the reversible capacity is 97 mAh g^{-1} at 10 C, 95 mAh g^{-1} at 20 C, 92 mAh g^{-1} at 30 C and 70 mAh g^{-1} at 50 C, respectively (Fig. 6a). Evidently, this excellent rate capability is due to the nanochain structure of the prepared $LiMn_2O_4$ particles, as it is well known that nanoparticles allow Li^+ ions to de-intercalate and intercalate very easily because of the very short diffusion distance [27]. Considering the relatively lower ionic conductivity of the $LiClO_4$ electrolyte in comparison with that of $LiPF_6$ electrolyte [28], this excellent rate capability and capacity of our

prepared nano $LiMn_2O_4$ has been very rarely reported. The capacity is a little higher with a good cycling life, which is not easy to achieve [29].

The nanochain $LiMn_2O_4$ cathodes also exhibit good cycling behavior. An important observation is that the reduction in discharge capacity after 50 cycles is remarkably low. We speculate that the nanochains can absorb/alleviate stress/strain during Li-ion de-/intercalation, preserving structural integrity of the cathode material [30–32]. The crystallinity of the nanochain $LiMn_2O_4$ is lower than the commercial material, which would provide more space to accommodate the possible strain or stress during the charge and discharge process [32]. Of course, the possible dissolution of Mn by acid such as HF formed from $LiPF_6$ does not happen in the $LiClO_4$ based electrolyte, which is similar to the cycling behavior in aqueous electrolytes [25,33].

4. Conclusion

Nanochain $LiMn_2O_4$ was prepared using a starch-assisted sol–gel method. Its crystallinity is lower than that of the commercial product. At the low charge and discharge rate of 1 C, it has a reversible capacity of 100 mAh g^{-1}. When it is charged and discharged at 20 C, the reversible capacity is still 58 mAh g^{-1} (58% of the normal capacity). When it is charged at 1 C and discharged at 50 C under the cut-off voltage of 3.0 V, the reversible capacity is 70 mAh g^{-1}. In addition, the primary cycling behavior is excellent and there is no evident capacity fading after 50 cycles. These microchain materials consisting of nanoparticles could be prepared by a simple method which could be more suitable in actual industry fabrication than unitary nanoparticles, while the reagglomeration of nanoparticles was avoided. All the advantages of nanomaterials could be conserved in a relatively wide range using this kind of material. This excellent electrochemical behavior is mainly due to the nanochain structure of the prepared $LiMn_2O_4$, and it provides new clues to the exploring of new high rate capability electrode materials, which is the key to the success of electric and hybrid electric vehicles (EVs and HEVs) technology.

Acknowledgements

Financial support from National Basic Research Program of China (973 Program No. 2007CB209702), International Science & Technology Cooperation Program of China (2010DFA61770), STCSM (09QH1400400) and NSFC (21073046) is gratefully acknowledged.

References

[1] B. Scrosati, Nature 373 (1995) 557.
[2] E. Hosono, T. Kudo, I. Honma, H. Matsuda, H. Zhou, Nano lett. 9 (2009) 1045.
[3] Y.P. Wu, X.B. Dai, J.Q. Ma, Y.J. Cheng, Lithium Ion Batteries: Practice and Applications, Chemical Industry Press, Beijing, 2004.
[4] K. Kang, Y.S. Meng, J. Breger, C.P. Grey, G. Ceder, Science 311 (2006) 977.
[5] A.S. Arico, P. Bruce, B. Scrosati, J.E. Tarascon, W. van Schalkwijk, Nat. Mater. 4 (2005) 366.
[6] L. Taberna, S. Mitra, P. Poizot, P. Simon, J.M. Tarascon, Nat. Mater. 5 (2006) 567.
[7] J.H. Choy, D.H. Kim, C.W. Kwon, S.J. Hwang, Y.I. Kim, J. Power Sources 77 (1999) 1.
[8] A.K. Padhi, K.S. Nanjundaswamy, J.B. Goodenough, J. Electrochem. Soc. 144 (1997) 1188.
[9] G. Amatucci, J.M. Tarascon, J. Electrochem. Soc. 149 (2002) K31.
[10] Y. Xia, T. Sakai, T. Fujieda, X.Q. Yang, X. Sun, Z.F. Ma, J. McBreen, M. Yoshio, J. Electrochem. Soc. 148 (2001) A723.
[11] Y. Shin, A. Manthiram, Chem. Mater. 15 (2003) 2954.
[12] H.Y. Jang, H.K. Jung, Y.K. Hye, N.K. You, C.K. Yun, J.H. Lee, J. Power Sources 196 (2011) 2858.
[13] K.M. Shaju, P.G. Bruce, Chem. Mater. 20 (2008) 5557.
[14] P.Z. Shen, D.Z. Jia, Y.D. Huang, L. Liu, Z.P. Guo, J. Power Sources 158 (2006) 608.
[15] H.W. Lee, P. Muralidharan, R. Ruffo, C.M. Mari, Y. Cui, D.K. Kim, Nano Lett. 10 (2010) 3852.
[16] M.W. Raja, S. Mahanty, R.N. Basu, J. Mater. Chem. 19 (2009) 6161.
[17] X.M. Liu, Z.D. Huang, S. Oh, P.C. Ma, P.C.H. Chan, G.K. Vedam, K. Kang, J.K. Kim, J. Power Sources 195 (2010) 4290.
[18] P. Lucas, C.A. Angell, J. Electrochem. Soc. 147 (2000) 459.
[19] S.H. Kang, J.B. Goodenough, L.K. Rabenbarg, Electrochem. Solid-State Lett. 4 (2001) A49.
[20] Y.S. Horn, S.A. Hackney, A.J. Kahaian, K.D. Kelper, E. Skinner, J.T. Voughey, M.M. Thackeray, J. Power Sources 81 (1996) 496.
[21] N.C. Li, C.J. Patrissi, G.L. Che, C.R. Martin, J. Electrochem. Soc. 147 (2000) 2044.
[22] H.S. Zhou, D.L. Li, M. Hibino, I. Honma, Angew. Chem. Int. Ed. 44 (2005) 797.
[23] I. Moriguchi, R. Hidaka, H. Yamada, T. Kudo, H. Murakami, N. Nakashima, Adv. Mater. 18 (2006) 69.
[24] W. Tang, L.L. Liu, S. Tian, L. Li, Y.B. Yue, Y.P. Wu, S.Y. Guan, K. Zhu, Electrochem. Commun. 12 (2010) 1524.
[25] W. Tang, S. Tian, L.L. Liu, L. Li, H.P. Zhang, Y.B. Yue, Y. Bai, Y.P. Wu, K. Zhu, Electrochem. Commun. 13 (2011) 205.
[26] Y.P. Wu, E. Rahm, R. Holze, Electrochim. Acta 47 (2002) 3491.
[27] Y.G. Guo, Y.S. Hu, W. Sigle, J. Maier, Adv. Mater. 19 (2007) 2087.
[28] G. Moumouziasa, G. Ritzoulis, D. Siapkas, D. Terzidis, J. Power Sources 122 (2003) 57.
[29] Y.C. Chen, K. Xie, Y. Pan, C. Zheng, J. Power Sources 15 (2011) 6493.
[30] L.C. Yang, Q.S. Gao, Y.H. Zhang, Y. Tang, Y.P. Wu, Electrochem. Commun. 10 (2008) 118.
[31] Q.T. Qu, P. Zhang, B. Wang, Y.H. Chen, S. Tian, Y.P. Wu, R. Holze, J. Phys. Chem. C 113 (2009) 14020.
[32] L.C. Yang, Q.T. Qu, Y. Shi, Y.P. Wu, T. van Ree, in: Małgorzata Sopicka-Lizer (Ed.), High Energy Ball Milling: Mechanochemical Production of Nanopowders, Woodhead Publishing Limited, Oxford, 2010, p. 372.
[33] Q.T. Qu, L.J. Fu, X.Y. Zhan, D. Samuelis, L. Li, W.L. Guo, Z.H. Li, Y.P. Wu, J. Maier, Energ. Environ. Sci. 4 (2011), doi:10.1039/c0ee00673d.
[34] C.H. Lu, S.K. Saha, J. Sol–Gel Sci. Technol. 20 (2001) 27.
[35] R. Thirunakaran, A. Sivashanmugan, S. Gopukumar, C.W. Dunnill, D.H. Gregory, J. Phys. Chem. Solids 69 (2008) 2082.
[36] L. Tian, A. Yuan, J. Power Sources 192 (2009) 693.